Society of Medical Education & Research

2026, Volume 6, Issue 1, Page No: 188-206
ISSN: 3108-4834

Archive of International Journal of Cancer and Allied Science

The Clinical and Biological Role of FBLN5 in Gastric Cancer

Yifan Zhao[1]*, Liang Chen[1], Ahmad Fauzi[2], Nor Hayati[3]

[1]Department of Gastric Cancer and Tumor Biology, Faculty of Medicine, China Agricultural University, Beijing, China.
[2]Department of FBLN5 and Clinical Significance, Faculty of Medicine, University of Malaya, Kuala Lumpur, Malaysia.
[3]Department of Biological Role and Translational Research, Faculty of Medicine, Universiti Putra Malaysia, Serdang, Malaysia.

***E-mail** ✉ yifan.zhao@cau.edu.cn

Abstract

Irregular expression of FBLN5 has been linked to different forms of cancer. The present study represents the initial investigation into its clinical and functional importance in gastric cancer (GC). Using data from The Cancer Genome Atlas-GC (TCGA-GC) and Gene Expression Omnibus (GEO) databases, we identified differences in FBLN5 expression and examined its association with clinicopathological features. Survival analysis via a Kaplan–Meier plotter evaluated FBLN5's influence on patient prognosis, while its biological roles were also explored. Furthermore, we developed a GC tissue microarray and conducted immunohistochemical staining for FBLN5 to validate the results. Western blotting was performed in parallel to establish FBLN5 overexpression in GC. We observed that elevated FBLN5 mRNA levels in GC were associated with an unfavorable prognosis. Increased FBLN5 expression showed notable associations with INFc and N3 lymph node metastasis. Both univariate and multivariate analyses identified FBLN5 expression and lymph node metastasis rate as independent prognostic risk factors for GC patients. These factors can be integrated to generate a nomogram for clinical use. Overall, FBLN5 shows a strong association with poorer outcomes in GC patients and serves as a useful prognostic marker.

Keywords: Prognosis, Gastric cancer, Fibroblast, FBLN5

Introduction

Gastric cancer (GC) ranks as the second most frequent malignancy of the digestive system and the third primary contributor to cancer-related mortality globally [1]. Early detection rates remain low, with approximately 70% of cases identified at an advanced stage [2]. In advanced GC, the majority of tumor cells have already penetrated blood or lymphatic vessels [3]. These cells can remain dormant and establish themselves at distant sites, leading to a 20% recurrence rate even 5 years after radical surgery among patients with lymph node metastasis, with a hematogenous metastasis rate reaching 40% [4]. The tumor microenvironment (TME) in GC is multifaceted, featuring intricate interactions between tumor cells and surrounding stromal elements. For instance, fibroblasts within the TME contribute to tumor angiogenesis [5]. They can also trigger epithelial-mesenchymal transition (EMT), activate RAS and transforming growth factor-beta (TGF-β) pathways, prompting tumor cells to adopt a mesenchymal phenotype and downregulate E-cadherin. This diminishes cell-cell adhesion [6, 7], enabling cancer cells to detach from the primary tumor and disseminate through the bloodstream, thereby facilitating distant spread [8]. Additionally, fibroblasts modulate immune cell recruitment, characteristics, and spatial distribution in the TME via multiple mediators, including

Access this article online https://smerpub.com/

Received: 07 March 2026; **Accepted:** 08 June 2026

Copyright CC BY-NC-SA 4.0

How to cite this article: Zhao Y, Chen L, Fauzi A, Hayati N. The Clinical and Biological Role of FBLN5 in Gastric Cancer. Arch Int J Cancer Allied Sci. 2026;6(1):188-206. https://doi.org/10.51847/VUGAWqjfk3

chemokines (CXCL12 and CXCL16), interleukins (IL6, IL8, and IL11), and surface proteins (PD-1 and PD-2). Such modulation can suppress anti-tumor immunity and enhance the metastatic potential of tumor cells [9].

While cancer-associated fibroblasts have been investigated using bioinformatics and experimental methods, the contributions of specific fibroblast subtypes in tumors remain unclear. The fibulin (FBLN) family, comprising fibulins 1–7, is prevalent in the extracellular matrix (ECM) and participates in basement membrane assembly, elastic fiber stabilization, and connective tissue organization [10, 11]. Distinct from other family members, FBLN5 possesses a conserved RGD motif that interacts with integrins to support endothelial cell attachment [12, 13]. This protein is crucial for the assembly of continuous elastin (ELN) polymers and for facilitating microfibril-ELN interactions [14]. In various physiological contexts, FBLN5 influences cell growth, movement, tumor formation, and tissue regeneration [15]. It also acts as a downstream target of TGF-β signaling in fibroblasts and endothelial cells [16, 17], thereby impacting tumor development. The existing literature indicates that FBLN5 can suppress or enhance tumor progression depending on the cancer context. In ovarian cancer, it promotes cell cycle arrest and modulates cycle-related proteins, thereby hindering cancer advancement and spread [15]. Similar tumor-suppressive activity has been observed in bladder cancer [18] and lung cancer [19]. Conversely, FBLN5 drives EMT and upregulates matrix metalloproteinase activity, fostering metastasis in breast cancer [20]. It similarly promotes metastatic processes in pancreatic cancer [21], cervical cancer [22], and GC. Prior studies on FBLN5 in GC [23, 24] have indicated its elevated expression in advanced stages and its capacity to enhance GC cell proliferation and invasion. Nevertheless, the clinical relevance and mechanistic roles of FBLN5 in GC have remained largely undefined until now; this study therefore addresses these gaps.

Materials and Methods

Patients and tissue samples

Tumor tissues, matched normal adjacent tissues, and corresponding clinical information were gathered from 269 GC patients who received radical gastrectomy at Harbin Medical University (HMU) Cancer Hospital. These resources formed the HMU-GC cohort, with follow-up data refreshed through December 2021. All specimens were obtained following written informed consent. The protocol received Institutional Review Board approval from the Affiliated Cancer Hospital of Harbin Medical University. The datasets are deposited in the GEO repository under accessions GSE184336 and GSE179252. RNA extraction, library preparation, and mRNA sequencing were carried out by Novogene Biotech Co., Ltd. (Beijing, China).

Data processing

High-throughput sequencing data from The Cancer Genome Atlas-Stomach Adenocarcinoma (TCGA-STAD) and the HMU-GC cohort were normalized for gene length and sequencing depth, then expressed as transcripts per kilobase million (TPM) values. Batch effects arising from non-biological sources were adjusted using the ComBat algorithm (22257669) implemented in the "sva" package. The merged HMU-GC and TCGA-STAD datasets served as the training cohort. For GEO microarray datasets GSE15459 and GSE62254, raw CEL files were processed to obtain absolute mRNA expression values and, similarly, batch effects were corrected with ComBat (22257669), forming the validation cohort.

Bioinformatics analyses

Within the training cohort, patients were stratified into high- and low-FBLN5 mRNA expression groups based on the median. Principal component analysis (PCA) was conducted after z-score normalization of the expression matrix, followed by dimensionality reduction using the prcomp function. Differentially expressed genes between the groups were identified with the "limma" package, applying thresholds of fold change ≥ 2, p-value < 0.05, and false discovery rate (FDR) adjustment. Gene ontology (GO) enrichment was performed for molecular function (MF), cellular component (CC), and biological process (BP) categories using annotations from the "org.Hs.eg.db" package. For Kyoto Encyclopedia of Genes and Genomes (KEGG) pathway analysis, updated pathway annotations were retrieved via the KEGG REST API (https://www.kegg.jp/kegg/rest/keggapi.html) and analyzed with the "clusterProfiler" package (accessed 7 April 2022). Gene set enrichment analysis (GSEA) via "clusterProfiler" identified enriched pathways in the high-expression group against hallmark gene sets, with criteria of |normalized enrichment score (NES)| > 1, nominal p-value < 0.05, and FDR q-value < 0.25. Protein-protein interaction (PPI) networks were

constructed using the STRING database version 11.5 (https://string-db.org), with a minimum interaction score of 0.9 (accessed 10 November 2021). Receiver operating characteristic (ROC) curves and time-dependent ROC analyses were generated with the "pROC" and "timeROC" packages and visualized with "ggplot2". Risk factor plots were also produced with "ggplot2". Immune infiltration relationships with FBLN5 expression were evaluated using CIBERSORT and TIMER algorithms. The ESTIMATE algorithm quantified immune and stromal cell content, yielding immune scores, stromal scores, and tumor purity estimates. Somatic mutation data for TCGA-STAD were acquired via the GDCquery_Maf() function (Mutect2 pipeline) from the "TCGAbiolinks" package and visualized with "maftools" to highlight the top 20 most frequently mutated genes across expression groups. Drug sensitivity predictions relied on the PRISM repository. FBLN5's potential as an immunotherapy biomarker was assessed through the Tumor Immune Dysfunction and Exclusion (TIDE) database (http://tide.dfci.harvard.edu/; accessed 11 June 2021). Single-sample gene set enrichment analysis (ssGSEA) was employed to compute EMT scores for individual samples. Nomograms and calibration plots were developed using the "rms" and "survival" packages, while decision curve analysis (DCA) utilized the "survival" package and the stdca.R script. These bioinformatics procedures were supported by Sangerbox 3.0, version 1.1.3 (Yongxin Liu, Shenzhen, China) [25].

Immunohistochemistry

A total of 180 human GC tissue specimens from Harbin Medical University Cancer Hospital were selected. Following tissue processing, embedding, sectioning, and hematoxylin-eosin (HE) staining, a tissue microarray (TMA) was assembled. The TMA slides were baked at 62 °C for 2 hours, dewaxed in xylene, rehydrated through graded alcohols, and subjected to antigen retrieval in EDTA buffer (pH 7.4) at 120 °C for 3 minutes, followed by natural cooling. Endogenous peroxidase was quenched with 0.3% hydrogen peroxide in methanol for 30 minutes. Slides were washed three times in PBS (10 minutes each), blocked with goat serum for 1 hour at room temperature, and incubated overnight at 4 °C (up to 16 hours) with FBLN5 rabbit polyclonal antibody (ABclonal, Woburn, MA, USA) diluted 1:150. The following day, secondary antibodies were applied for 40 minutes at room temperature in a humidified chamber. Visualization was achieved with diaminobenzidine (DAB), followed by hematoxylin counterstaining and bluing with ammonia. Two experienced pathologists independently scored all slides. Digital scanning was performed at 200× magnification using a Leica DM4B microscope (Leica Microsystems GmbH, Wetzlar, Germany). Staining intensity was semi-quantitatively evaluated via the H-score (range 0–300), calculated as staining intensity (0 = negative, 1 = weak, 2 = moderate, 3 = strong) multiplied by the percentage of positively stained area. High- and low-expression groups were determined based on survival outcomes using X-tile software.

Western blotting

Cells from various lines (GES, AGS, BGC-823, HGC-27, and MKN-28) were harvested and lysed on ice using RIPA buffer supplemented with phosphatase and protease inhibitors for 30 minutes. Following centrifugation at 13,000 rpm for 15 minutes, the supernatant was carefully collected, and the cellular debris was discarded. An appropriate volume of 5× loading buffer was then added, and the samples were boiled at 100 °C for 10 minutes. Protein concentrations were quantified with the BCA assay kit (Thermo Scientific, Waltham, MA, USA). Equal amounts of protein were separated by 12% SDS-PAGE and transferred onto PVDF membranes under cold conditions. Membranes were blocked with 5% non-fat milk for 2 hours, followed by overnight incubation at 4 °C with primary antibodies (FBLN5 at 1:1000 dilution, ABclonal, USA; β-Tubulin at 1:1000 dilution, ABclonal, USA). The next day, membranes were incubated for 1 hour with horseradish peroxidase-conjugated secondary antibody (1:5000). Protein bands were visualized using the ECL detection kit (Thermo Scientific, USA). All experiments were repeated three times.

Statistical analyses

All statistical analyses were conducted using SPSS version 25.0. The Kruskal–Wallis test was applied for comparisons involving continuous variables, whereas the Chi-square test assessed associations between FBLN5 mRNA or protein expression and patients' clinicopathological parameters. Hazard ratios (HRs) with 95% confidence intervals (CIs) were calculated using Cox proportional hazards regression in the survival package. Kaplan–Meier curves were generated for survival analysis. A two-sided p-value below 0.05 was

regarded as statistically significant throughout the analyses.

Results and Discussion

Associations of FBLN5 mRNA expression with prognosis and clinicopathological characteristics

Patients were stratified into high- and low-FBLN5 mRNA expression groups using the median expression value as the cutoff. Principal component analysis (PCA) confirmed satisfactory intra-group homogeneity and inter-group separation **(Figure 1a)**. Individuals in the high-expression group exhibited markedly inferior survival outcomes, with a median survival time of 33.03 months compared to 68.37 months in the low-expression group (P < 0.001, HR: 1.60, 95% CI: 1.25–2.05) **(Figure 1b)**. Consistent with the validation cohort, the high-FBLN5 expression group likewise displayed a significantly worse prognosis relative to the low-expression group (P < 0.001, HR = 0.63, 95% CI: 0.49–0.81) **(Figure 1c)**. Further assessment using TCGA data revealed poorer disease-specific survival (DSS) **(Figure 1d)** and progression-free interval (PFI) **(Figure 1e)** among patients with elevated FBLN5 levels. Comparison of FBLN5 expression between tumor tissues and matched adjacent normal tissues in the training cohort demonstrated substantially higher levels in cancerous tissues **(Figure 1f)**. Correlation analyses with clinical variables indicated that FBLN5 mRNA expression was independent of patient sex and M stage, but showed strong positive associations with T stage **(Figure 1g)** (P < 0.001), N stage **(Figure 1h)** (P < 0.001), and overall pTNM stage **(Figure 1i)** (P < 0.001).

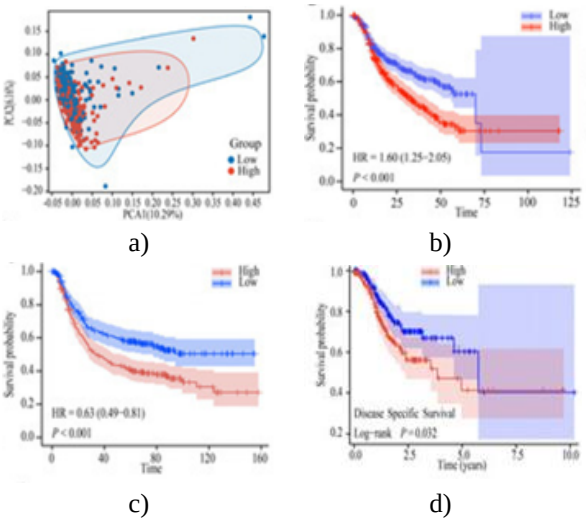

a) b) c) d)

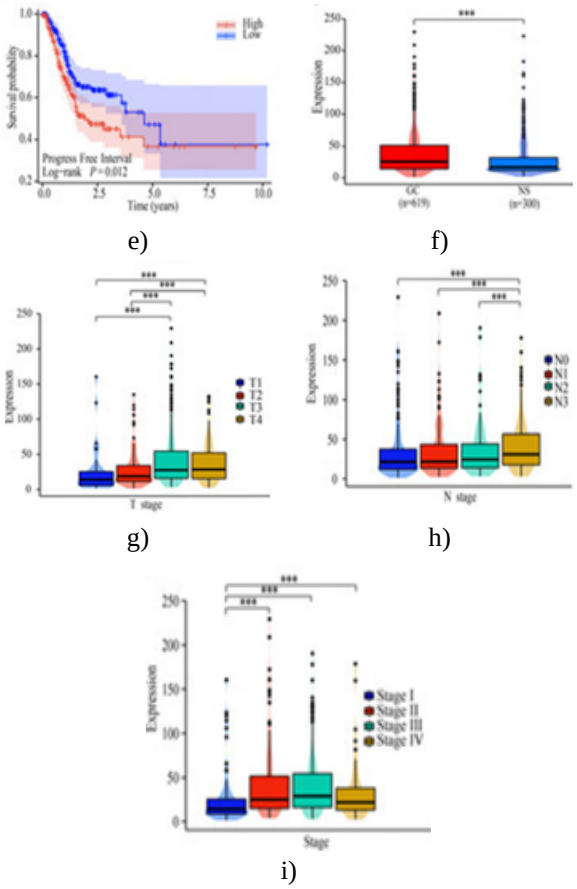

e) f) g) h) i)

Figure 1. Links between FBLN5 mRNA levels and patient survival outcomes along with clinical and pathological traits

(a) Principal component analysis (PCA) illustrating the separation and consistency of patient groups stratified by FBLN5 expression, (b) Kaplan–Meier plot depicting overall survival differences between high- and low-FBLN5 expression cohorts in the merged HMU-TCGA dataset (P < 0.001), (c) Overall survival curves for high- versus low-FBLN5 expression patients in the GEO validation set (P < 0.001), (d) Disease-specific survival (DSS) comparison across high- and low-FBLN5 groups (P < 0.05), (e) Progression-free interval (PFI) evaluation in the high- versus low-expression categories (P < 0.05), (f) Comparison of FBLN5 expression in gastric cancer samples (619 cases) relative to corresponding normal tissues (300 cases), and (g–i) FBLN5 mRNA levels according to varying disease stages in GC cases (P < 0.05). ***P < 0.001 (HMU, Harbin Medical University; TCGA, The Cancer Genome Atlas; GEO, Gene Expression Omnibus; GC, gastric cancer; DSS, disease-specific survival; PFI, progression-free interval).

Functional roles of FBLN5 in biology

Using limma-based differential gene expression analysis, we detected 2663 genes showing increased expression and 5957 genes with decreased expression linked to FBLN5 **(Figure 2a)**. GO enrichment analysis of these genes revealed that FBLN5, along with its associated genes, contributes to multiple biological processes (BPs), including system development, negative regulation of cellular activities, cell differentiation, modulation of signaling pathways, phosphorus metabolism, and cellular responses to chemical cues **(Figure 2b)**. Regarding cellular components (CCs), notable enrichment occurred in the cytosol, nuclear regions, vessels, intelligent vessels, and cyclomatic vessels **(Figure 2c)**. Molecular functions (MFs) highlighted involvement in cytoskeletal protein interactions, transcription factor attachment, cell adhesion molecule recognition, GTPase activity, and small GTPase binding **(Figure 2d)**.

Pathway analysis through KEGG indicated primary participation of FBLN5-related elements in the MAPK, Rap1, and cGMP-PKG cascades **(Figure 2e)**. Results from gene set enrichment analysis (GSEA) demonstrated prominent activation of pathways associated with EMT, TGF-β signaling, programmed cell death, hypoxic conditions, and new blood vessel formation in samples with elevated FBLN5 **(Figure 2f)**.

A protein-protein interaction (PPI) network was generated, revealing direct interactions among FBLN5, LOX, LOXL1, LOXL2, LOXL3, LOXL4, and ELN **(Figure 2g)**. We further examined the prognostic utility of proteins within this PPI network. By integrating mRNA expression data of these molecules with routine clinical and pathological indicators, a risk prediction model was formulated. Individual ROC assessments were conducted to gauge the standalone prognostic performance of FBLN5, ELN, LOX, LOXL1, LOXL2, LOXL3, and LOXL4 **(Figures 3a–3g)**. Since single-gene models offered only modest predictive power, Cox regression was utilized to identify genes with independent prognostic value. This process pinpointed FBLN5, ELN, and LOX as key contributors. A combined prognostic risk score was calculated from the expression levels of FBLN5, ELN, and LOX, which showed greater stability and reliability than any single gene **(Figure 3h)**. Survival analysis via the Kaplan–Meier method showed markedly inferior overall survival (OS) for patients assigned higher risk scores **(Figure 3i)**. A visual risk nomogram plot was created to display the model's distribution trends, featuring expression patterns of FBLN5, ELN, and LOX **(Figure 3j)**. Ultimately, the risk score was combined with established clinicopathological variables in a multivariate Cox analysis, yielding a comprehensive prognostic nomogram **(Figure 3k)**. Subsequent ROC analysis confirmed that the nomogram integrating the risk score, pTNM staging, and patient age provided improved predictive capability for GC patient outcomes **(Figure 3l)**.

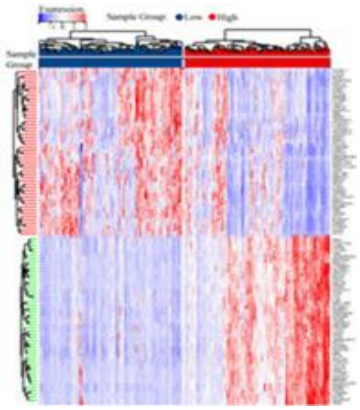

a)

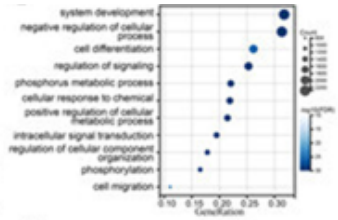

b)

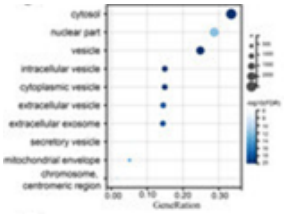

c)

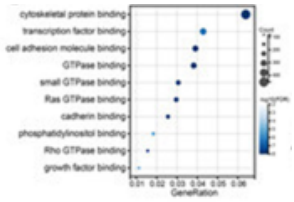

d)

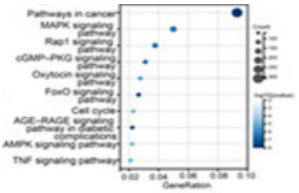

e)

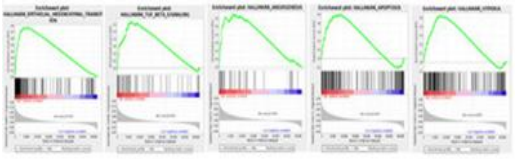

f)

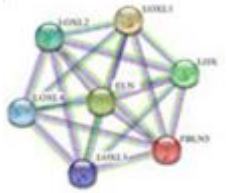

g)

Figure 2. Investigation into the molecular and cellular roles performed by FBLN5

(a) Detection of genes with differential expression between patient groups with high versus low FBLN5 levels, using the limma tool. Illustrative gene ontology (GO) enrichment outcomes from the TCGA-GC dataset for high- compared to low-FBLN5-expressing samples, encompassing: (b) Biological processes (BP) relevant to the functional contributions of FBLN5, (c) Cellular components (CC) implicated in FBLN5 actions, (d) Molecular functions (MF) connected with FBLN5 gene activity. (e) Typical KEGG pathway enrichment findings contrasting the high- and low-FBLN5 expression categories using TCGA-GC information. (f) Gene set enrichment analysis (GSEA) performed on samples from the high-FBLN5 expression category highlighting hypoxia, angiogenesis, TGF-β, EMT, and apoptosis-related gene sets (meeting ALL |normalized enrichment score (NES)| > 1, nominal (NOM) P-value < 0.05, and FDR q-value < 0.25 thresholds). (g) Examination of the protein-protein interaction (PPI) network involving partners linked to FBLN5.

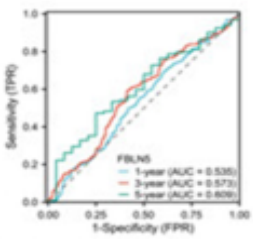

a)

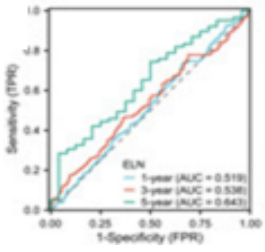

b)

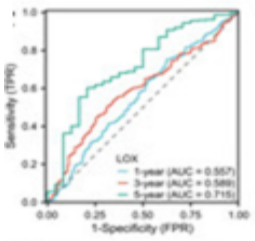

c)

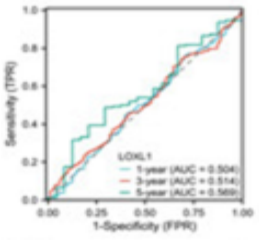

d)

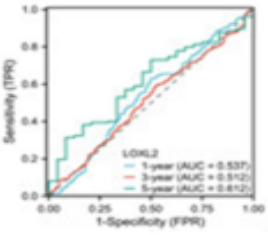

e)

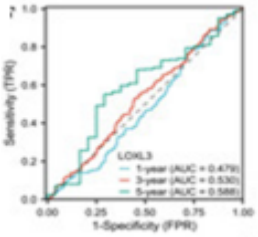

f)

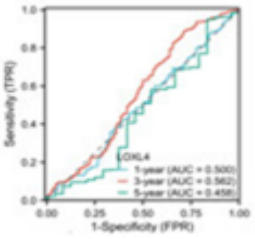

g)

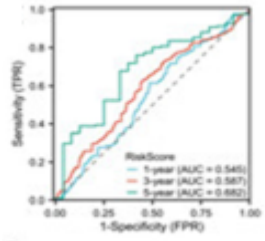

h)

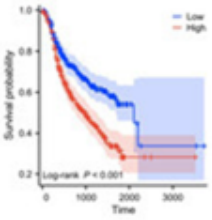

i)

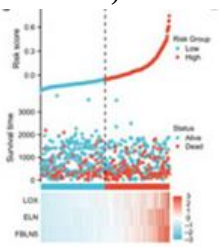

j)

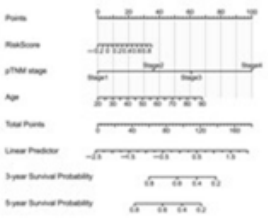

k)

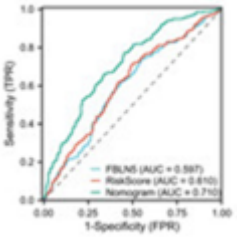

l)

Figure 3. Estimation of survival prospects in gastric cancer cases utilizing FBLN5 mRNA abundance

(a–g) Receiver operating characteristic (ROC) curves examining the predictive performance of mRNA levels for prognosis of FBLN5, ELN, LOX, LOXL1, LOXL2, LOXL3, and LOXL4, (h) Integrated prognostic risk index formulated from FBLN5, ELN, and LOX

expression values, (i) Analysis of patients' overall survival (OS) according to categories defined by the prognostic risk index, (j) Graphical representation highlighting patterns and distributions in the developed prognostic scoring system, (k) Nomogram designed for outcome prediction incorporating the risk index, pTNM classification, and age, and (l) ROC evaluation comparing FBLN5 expression level, the composite risk index, and the complete nomogram approach (OS: overall survival).

Associations between FBLN5 expression and immune characteristics

Analyses were conducted to examine the interplay between FBLN5 expression and the tumor microenvironment's immune composition. CIBERSORT assessment, displayed in **Figure 4a**, demonstrated clear links between higher FBLN5 and altered infiltration levels of CD4+ T cells, NK cells, M0 macrophages, M2 macrophages, mast cells, and multiple other immune populations (all $P < 0.05$). Results from TIMER further confirmed meaningful variations in CD4+ T cell, CD8+ T cell, neutrophil, macrophage, and dendritic cell presence within the high-FBLN5-expressing tumors **(Figure 4b)** (all $P < 0.05$). Additionally, the high-expression category exhibited elevated estimate scores **(Figure 4c)**, immune scores **(Figure 4d)**, and stromal scores **(Figure 4e)**, while displaying decreased tumor purity **(Figure 4f)** (all $P < 0.05$). Collectively, these patterns underscore FBLN5's considerable impact on shaping the immune profile inside the tumor microenvironment.

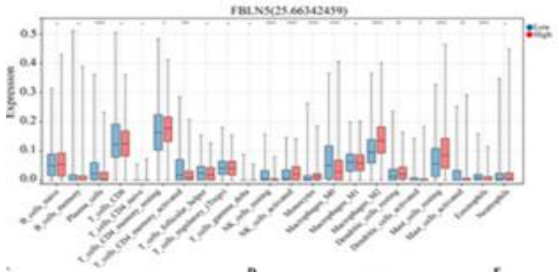

a)

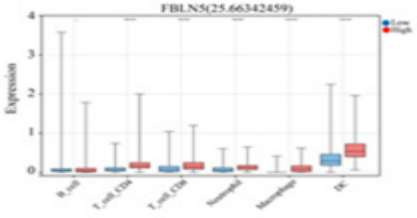

b)

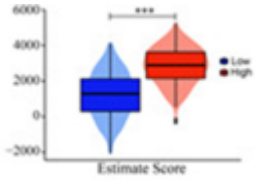

c)

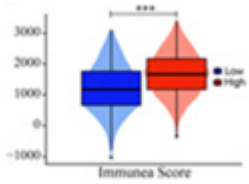

d)

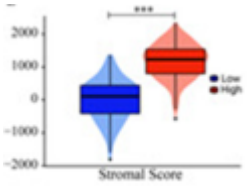

e)

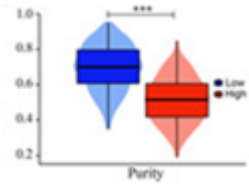

f)

Figure 4. Connections of FBLN5 with immune cell involvement

(a) CIBERSORT and (b) TIMER computational approaches were applied to initially determine associations between FBLN5 expression and immune cell infiltration across individual tumor specimens, The (c) ESTIMATE method quantified the presence of immune and stromal elements in gastric cancer, enabling calculation of the (d) immune score, (e) stromal score, and (f) tumor purity. * $P < 0.05$, ** $P < 0.01$, *** $P < 0.001$, **** $P < 0.0001$.

Linkage of FBLN5 to tumor advancement

We assessed how responsive GC patients might be to the chemotherapeutic agents irinotecan, 5-fluorouracil, docetaxel, capecitabine, paclitaxel, cisplatin, and oxaliplatin across varying FBLN5 expression levels. This revealed that FBLN5 levels influenced sensitivity specifically to capecitabine, cisplatin, and oxaliplatin **(Figure 5a)**. Concurrently, the potential of FBLN5 as an indicator for immunotherapy checkpoint responsiveness was examined **(Table 1)**. Furthermore, elevated EMT

scores were detected in the high-FBLN5 expression group relative to the low-expression group **(Figure 5b)**. This suggests that increased FBLN5 may facilitate the detachment of GC cells from the primary site and their dissemination to distant locations via the EMT mechanism, thereby supporting a tight connection between FBLN5 and tumor advancement.

Additionally, missense mutation analysis at the exon level was carried out **(Figure 5c)** by comparing high- and low-FBLN5 expression groups using TCGA-STAD data. Findings indicated a lower mutation frequency of FBLN5 within the high-expression cohort. This implies that FBLN5 contributes to stable control in individuals with advanced GC and maintains a strong association with disease progression in GC patients.

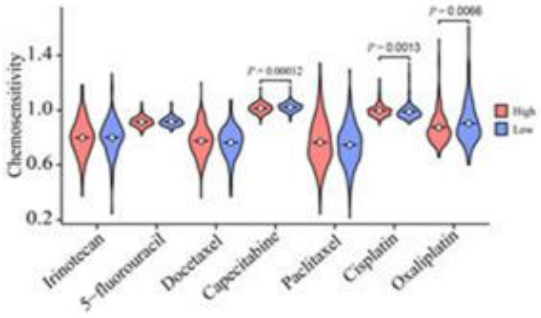

a)

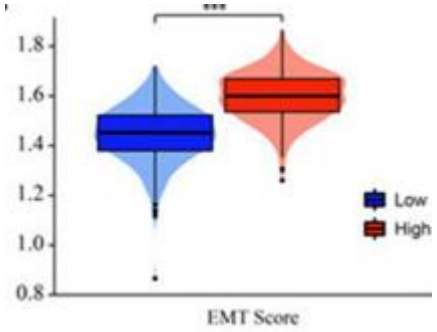

b)

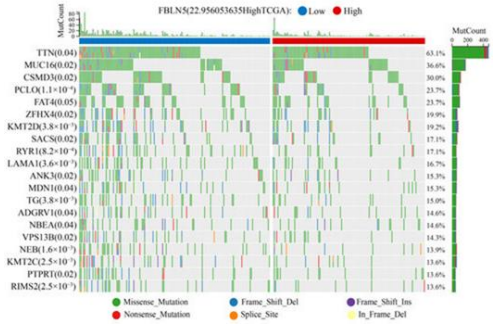

c)

Figure 5. Relationships between FBLN5 and tumor progression

(a) Chemotherapy analysis based on FBLN5 expression levels, (b) EMT score, (c) Mutations in FBLN5 during the regulation of cancer progression. *** P < 0.001.

Table 1. Predictive performance of FBLN5 for assessing sensitivity to immune checkpoint blockade using the TIDE framework

Study	Cancer Type	Treatment	Pos/Neg cases	AUC of TMB	AUC of CD8	AUC of CD274	AUC of FBLN5
Braun 2020	Kidney	PD1	201/94	0.56	0.60	0.56	0.58
Chen 2016	Melanoma	PD1_Prog	6/9	n/a	0.61	0.54	n/a
		CTLA4	5/11	n/a	0.67	0.42	n/a
Gide 2019	Melanoma	PD1	19/22	n/a	0.86	0.88	0.47
		PD1 + CTLA4	21/11	n/a	0.74	0.79	0.52
Hee 2020	NSCLC_Oncomine	PD1	9/12	n/a	0.56	0.45	n/a
Hugo 2016	Melanoma	PD1	14/12	0.68	0.49	0.60	0.28
Kim 2018	Gastric	PD1	12/33	n/a	0.80	0.88	0.19
Lauss 2017	Melanoma	ACT	10/15	0.76	0.71	0.78	0.69
Liu 2019	Melanoma	PD1_Prog	16/31	n/a	0.58	0.56	0.56
		PD1_Naive	33/41	n/a	0.47	0.51	0.39
Mariathasan 2018	Bladder_mUC	PD-L1	68/230	0.78	0.60	0.58	0.42
McDermott 2018	Kidney	PD-L1	20/61	0.54	0.66	0.62	0.60
Miao 2018	Kidney	ICB	20/13	0.65	0.47	0.42	0.67
Nathanson 2017	Melanoma	CTLA4_Pre	4/5	n/a	0.50	0.66	0.15
		CTLA4_Post	4/11	n/a	0.77	0.66	0.57
Prat 2017	NSCLC/HNSC/Melanoma	PD1	21/12	n/a	0.56	0.58	n/a

Riaz 2017	Melanoma	PD1_Prog	4/22	0.57	0.91	0.52	0.80
		PD1_Naive	6/19	0.62	0.43	0.27	0.54
Ruppin 2021	NSCLC	PD1	7/15	n/a	0.75	0.70	0.59
Uppaluri 2020	HNSC	PD1_Pre	8/15	n/a	0.58	0.69	0.37
		PD1_Post	9/13	n/a	0.48	0.70	0.23
VanAllen 2015	Melanoma	CTLA4	19/23	0.67	0.70	0.64	0.48
Zhao 2019	Glioblastoma	PD1_Pre	8/7	n/a	0.50	0.68	0.38
		PD1_Post	6/3		0.67	0.61	0.17

Abbreviation: TIDE = tumor immune dysfunction and exclusion.

FBLN5 protein levels and their impact on patient outcomes

To confirm the influence of FBLN5 on gastric cancer prognosis, immunohistochemical (IHC) staining for FBLN5 was conducted on the constructed tissue microarray **(Figure 6a)**. The staining pattern revealed predominant cytoplasmic localization of FBLN5 in malignant epithelial cells and stromal fibroblasts within the tumor. Distinct localization differences were noted between the high- and low-expression categories. In well-differentiated adenocarcinomas, strong cytoplasmic staining was evident in both cancer cells and tumor-associated fibroblasts. In poorly differentiated adenocarcinomas, FBLN5 was generally weakly expressed in tumor cells but remained strongly positive in interstitial fibroblasts. However, in some cases of poorly differentiated adenocarcinoma, cancer cells also showed strong cytoplasmic expression, highlighting heterogeneity in FBLN5 distribution even within tumors with comparable differentiation status. In mucinous adenocarcinoma, intense FBLN5 positivity was observed in the cytoplasm of cancer cells and surrounding fibroblasts.

Survival analysis based on IHC scores demonstrated markedly better overall survival (OS) in the low-expression group compared with the high-expression group ($P < 0.05$, HR = 2.40, 95 percent CI: 1.10–5.21) **(Figure 6b)**. Protein expression was additionally quantified in a normal gastric epithelial cell line and multiple GC cell lines **(Figure 6c)**, confirming significantly elevated FBLN5 levels in the cancerous lines. This suggests a potential association between FBLN5 abundance and GC histological subtypes.

Univariate and multivariate Cox proportional hazards analyses were performed to investigate further the association between FBLN5 expression and clinical prognosis **(Table 2)**. These analyses showed that FBLN5 expression and the rate of lymph node metastasis were independent predictors of patient outcome ($P < 0.05$). Chi-square testing additionally revealed associations between FBLN5 levels and both the tumor infiltration pattern (INF) and N stage. Individuals with high FBLN5 expression were more likely to present with the INFc infiltration pattern and N3 lymph node involvement **(Table 3)**.

A prognostic nomogram was subsequently developed incorporating the independent factors identified in the multivariate Cox model **(Figure 6d)**. Patients were stratified into high- and low-risk groups based on the median nomogram score, with the high-risk group exhibiting significantly shorter survival **(Figure 6e)**. Time-dependent ROC analysis yielded area under the curve (AUC) values of 0.751 (0.564–0.938) for 1-year, 0.769 (0.647–0.891) for 2-year, and 0.733 (0.612–0.855) for 3-year survival predictions **(Figure 6f)**. Calibration curves showed good agreement with a C-index of 0.705 (0.659–0.752) **(Figure 6g)**. Decision curve analysis (DCA) further supported the model's clinical utility **(Figure 6h)**. The DCA plots highlighted that combining FBLN5 expression with lymph node metastasis status provides significant prognostic value in GC patients.

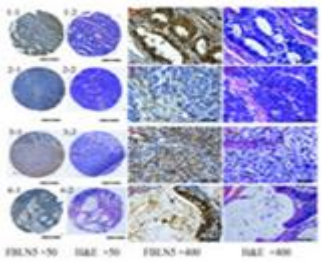

a)

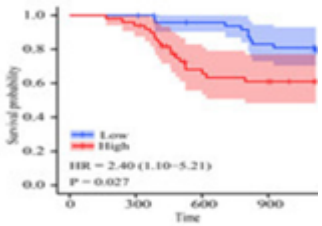

b)

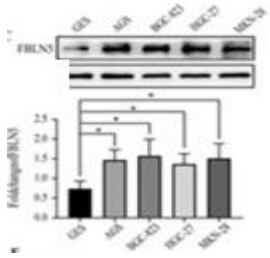

c)

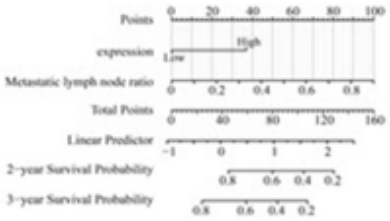

d)

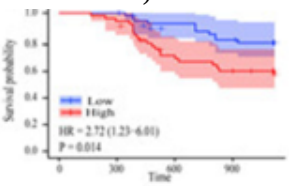

e)

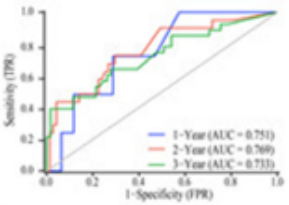

f)

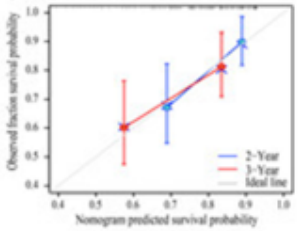

g)

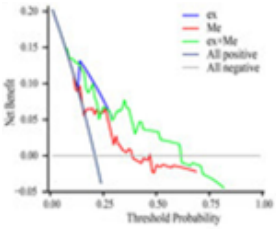

h)

Figure 6. Assessment of FBLN5 protein abundance and development of the prognostic scoring system

(a) Representative images of FBLN5 immunohistochemical staining together with H&E histology on the gastric cancer tissue microarray at ×50 and ×400 overall magnification. (A1) Well-differentiated adenocarcinoma showing strong FBLN5 positivity in the cytoplasm of tumor cells and in stromal fibroblasts. (A2) Poorly differentiated adenocarcinoma displaying weak cytoplasmic staining in cancer cells but prominent expression in interstitial fibroblasts. (A3) Separate case of poorly differentiated adenocarcinoma with strong FBLN5 expression. (A4) Mucinous adenocarcinoma exhibiting intense FBLN5 staining in the cytoplasm of cancer cells and surrounding fibroblasts. (b) Kaplan–Meier survival curves comparing patients with differing FBLN5 expression based on tissue microarray data. (c) Relative FBLN5 protein amounts across various cell lines (mean ± s.d.; number of replicates = 3). (d) Nomogram for outcome prediction incorporating FBLN5 expression status and lymph node metastasis rate. (e) Survival analysis stratified according to scores generated by the nomogram. (f) Receiver operating characteristic (ROC) curves evaluating the predictive reliability of the nomogram. (g) Calibration plots for two-year and three-year survival predictions. (h) Decision curve analysis (DCA) derived from FBLN5 expression combined with metastatic status. * P < 0.05.

Table 2. Cox univariate and multivariate analyses of FBLN5 gene expression.

Characteristics	Total (N)	Univariate analysis		Multivariate analysis	
		Hazard ratio (95% CI)	P-value	Hazard ratio (95% CI)	P-value
FBLN5 expression	100				
Low	50	Reference			
High	50	2.396 (1.102–5.205)	0.027	2.558 (1.162–5.632)	0.020
Sex	100				
Male	72	Reference			
Female	28	0.851 (0.362–2.002)	0.712		
Age	100	0.992 (0.957–1.028)	0.646		
BMI	100	0.944 (0.845–1.054)	0.303		
Tumor infiltration pattern	100				

INFa	20	Reference			
INFb	16	1.484 (0.371–5.937)	0.577		
INFc	48	1.761 (0.584–5.311)	0.315		
N/A	16	1.823 (0.489–6.790)	0.371		
Lymphatic infiltration	100				
Negative	55	Reference			
Positive	45	0.940 (0.445–1.988)	0.872		
Venous infiltration	100				
Negative	70	Reference			
Positive	30	0.592 (0.240–1.460)	0.255		
Nerve infiltration	100				
Negative	25	Reference			
Positive	75	2.243 (0.778–6.471)	0.135		
T stage	100				
T1	4	Reference			
T2	13	0.595 (0.054–6.565)	0.672		
T3	45	1.009 (0.130–7.821)	0.993		
T4	38	1.709 (0.225–12.999)	0.605		
pTNM stage	100				
I	10	Reference			
II	32	2.155 (0.259–17.902)	0.477		
III	58	4.558 (0.613–33.907)	0.138		
Metastatic lymph node ratio	100	14.056 (3.348–59.004)	< 0.001	7.133 (1.241–41.011)	0.028
Borrmann type	100				
I	7	Reference			
II	19	0.291 (0.041–2.068)	0.217		
III	68	1.003 (0.236–4.270)	0.997		
IV	6	1.214 (0.171–8.621)	0.847		
Postoperative chemotherapy	100				
Without	97	Reference			
With	3	1.211 (0.164–8.915)	0.851		
Tumor location	100				
Lower third	54	Reference			
Middle and Upper third	42	1.866 (0.847–4.113)	0.122	1.589 (0.676–3.734)	0.289
Entire stomach	4	7.426 (2.017–27.337)	0.003	2.869 (0.565–14.569)	0.204
Histological type	100				
Well to moderately differentiated	46	Reference			
Poorly differentiated	26	0.592 (0.215–1.629)	0.310		
Signet ring cell	20	1.126 (0.459–2.764)	0.795		
Mucinous	8	0.323 (0.043–2.447)	0.274		
HER2 expression	100				
Positive	18	Reference			
Negative	82	0.602 (0.256–1.418)	0.246		
CEA	100				
≤5 ng/mL	86	Reference			
>5 ng/mL	14	0.679 (0.205–2.250)	0.526		
CA-199	100				
≤37 U/mL	88	Reference			
>37 U/mL	12	1.745 (0.663–4.593)	0.260		
CA724	100				
≤6 U/mL	74	Reference			
>6 U/mL	26	1.096 (0.483–2.490)	0.826		
FBLN5	619	1.004 (1.001–1.007)	< 0.01	1.003 (0.998–1.007)	0.235
ELN	619	1.002 (1.000–1.003)	< 0.05	1.000 (0.998–1.003)	0.698
LOX	619	1.005 (1.001–1.009)	< 0.05	1.003 (0.998–1.008)	0.197
LOXL1	619	1.004 (0.999–1.009)	0.096		
LOXL2	619	1.002 (0.997–1.006)	0.499		

LOXL3	619	1.030 (0.992–1.069)	0.121		
LOXL4	619	1.012 (0.999–1.025)	0.062		< 0.05
RiskScore	619	2.718 (1.444–5.116)	< 0.01	2.226 (1.139–4.353)	
pTNM stage	605		< 0.001		
Stage 1	81	Reference		Reference	< 0.01
Stage 2	160	2.691 (1.395–5.191)	< 0.01	2.491 (1.287–4.823)	< 0.001
Stage 3	312	4.854 (2.633–8.947)	< 0.001	4.645 (2.510–8.596)	< 0.001
Stage 4	52	10.611 (5.412–20.806)	< 0.001	12.565 (6.368–24.793)	
Gender	619		0.371		
Female	221	Reference			
Male	398	1.123 (0.870–1.449)	0.373		
Age	616	1.017 (1.007–1.028)	< 0.01	1.025 (1.013–1.036)	< 0.001

BMI: body mass index. Tumor site, pattern of tumor invasion, venous invasion, and perineural invasion were determined based on postoperative pathological examination reports. INFa: expansive growth pattern featuring a clear demarcation from adjacent tissues; INFc: infiltrative growth pattern with an ill-defined border relative to surrounding tissues; INFb: intermediate growth pattern positioned between INFa and INFc. CEA: carcinoembryonic antigen; CA19-9: carbohydrate antigen 19-9; CA72-4: carbohydrate antigen 72-4. Measurements of CEA, CA19-9, and CA72-4 were obtained from tumor marker laboratory tests. Histological classification, Borrmann classification, and pTNM staging were performed according to the criteria outlined in the 8th edition of the AJCC staging system.

Table 3. Relationship between FBLN5 mRNA expression and clinical features of GC patients.

Characteristic	Low expression	High expression	P
n	64	116	
Sex, n (%)			0.066
Female	22 (12.2%)	24 (13.3%)	
Male	42 (23.3%)	92 (51.1%)	
Age, n (%)			0.173
< 60	25 (13.9%)	59 (32.8%)	
≥ 60	39 (21.7%)	57 (31.7%)	
BMI, n (%)			0.355
< 24	39 (21.7%)	80 (44.4%)	
≥ 24	25 (13.9%)	36 (20%)	
Tumor infiltration pattern, n (%)			0.037
INFa	17 (9.4%)	19 (10.6%)	
INFb	8 (4.4%)	36 (20%)	
INFc	27 (15%)	41 (22.8%)	
N/A	12 (6.7%)	20 (11.1%)	
Lymphatic infiltration, n (%)			0.050
Negative	43 (23.9%)	59 (32.8%)	
Positive	21 (11.7%)	57 (31.7%)	
Venous infiltration, n (%)			0.209
Negative	51 (28.3%)	81 (45%)	
Positive	13 (7.2%)	35 (19.4%)	
Nerve infiltration, n (%)			0.179
Negative	21 (11.7%)	26 (14.4%)	
Positive	43 (23.9%)	90 (50%)	
T stage, n (%)			0.241
T1	4 (2.2%)	6 (3.3%)	
T2	13 (7.2%)	14 (7.8%)	
T3	26 (14.4%)	42 (23.3%)	
T4	21 (11.7%)	54 (30%)	
N stage, n (%)			0.046
N0	25 (13.9%)	25 (13.9%)	
N1	12 (6.7%)	24 (13.3%)	

N2	9 (5%)	32 (17.8%)	
N3	18 (10%)	35 (19.4%)	
pTNM stage, n (%)			0.065
I	13 (7.2%)	10 (5.6%)	
II	20 (11.1%)	36 (20%)	
III	31 (17.2%)	70 (38.9%)	
Metastatic lymph node ratio, n (%)			0.510
<0.3	53 (29.4%)	87 (48.3%)	
≥0.6	3 (1.7%)	9 (5%)	
0.3≥, <0.6	8 (4.4%)	20 (11.1%)	
Borrmann type, n (%)			0.187
1	7 (3.9%)	8 (4.4%)	
2	17 (9.4%)	32 (17.8%)	
3	38 (21.1%)	62 (34.4%)	
4	2 (1.1%)	14 (7.8%)	
Postoperative chemotherapy, n (%)			1.000
With	1 (0.6%)	3 (1.7%)	
Without	63 (35%)	113 (62.8%)	
Tumor location, n (%)			0.780
Entire stomach	2 (1.1%)	4 (2.2%)	
Lower third	32 (17.8%)	65 (36.1%)	
Middle and Upper third	30 (16.7%)	47 (26.1%)	
Histological type, n (%)			0.079
Mucinous	5 (2.8%)	13 (7.2%)	
Poorly differentiated	11 (6.1%)	33 (18.3%)	
Signet ring cell	11 (6.1%)	26 (14.4%)	
Well to moderately differentiated	37 (20.6%)	44 (24.4%)	
HER2 expression, n (%)			1.000
Negative	55 (30.6%)	100 (55.6%)	
Positive	9 (5%)	16 (8.9%)	
CEA, n (%)			0.434
> 5 ng/mL	6 (3.3%)	17 (9.4%)	
≤ 5 ng/mL	58 (32.2%)	99 (55%)	
CA-199, n (%)			0.114
> 37 U/mL	4 (2.2%)	18 (10%)	
≤ 37 U/mL	60 (33.3%)	98 (54.4%)	
CA724, n (%)			1.000
> 6 U/mL	17 (9.4%)	30 (16.7%)	
≤ 6 U/mL	47 (26.1%)	86 (47.8%)	

Body mass index is denoted as BMI. Information on tumor site, infiltration pattern, venous invasion, and perineural invasion was derived from the postoperative pathology report. INFa indicates expansive growth with a well-defined interface relative to nearby tissues, INFc denotes infiltrative growth with an ill-defined border against surrounding tissue, and INFb represents an intermediate form between INFa and INFc. CEA stands for carcinoembryonic antigen, CA19-9 for carbohydrate antigen 19-9, and CA72-4 for carbohydrate antigen 72-4. Levels of CEA, CA19-9, and CA72-4 were obtained from the tumor marker assay. Histological type, Borrmann type, and pTNM stage were classified according to the 8th AJCC system.

FBLN5 in other cancers

The findings described earlier indicate that FBLN5 may serve as a reliable prognostic marker for patients with gastric cancer. To determine whether FBLN5 could similarly function as a prognostic factor in other malignancies, we examined its expression levels across multiple cancer types alongside corresponding survival outcomes. The results revealed that FBLN5 expression was also associated with prognosis in hepatocellular carcinoma, suggesting that its potential clinical utility in this cancer warrants further investigation **(Figures 7a and 7b)**.

We also assessed the relationship between FBLN5 expression and immune cell infiltration across various cancers utilizing TIMER and CIBERSORT analyses. TIMER results showed a positive association between FBLN5 and immune infiltration across most tumor types

(Figure 7c). In contrast, CIBERSORT analysis indicated a negative correlation between FBLN5 and immune activity in most tumors **(Figure 7d)**. Consequently, the precise role of FBLN5 in modulating immune infiltration across different cancers requires further detailed examination.

Additionally, evaluation of immune checkpoint molecules showed that FBLN5 expression was positively correlated with several immune checkpoints in many carcinomas, including lung adenocarcinoma (LUAD), bladder urothelial carcinoma (BLCA), and lung squamous cell carcinoma (LUSC). These associations may help inform the selection of appropriate immunotherapy strategies for these cancers **(Figure 7e)**.

Lastly, we investigated the broader pan-cancer potential of FBLN5 in targeted therapy through tumor purity analysis **(Figure 7f)**, tumor mutational burden (TMB) analysis **(Figure 7g)**, and microsatellite instability (MSI) analysis **(Figure 7h)**. These analyses found that higher FBLN5 expression tended to correlate negatively with TMB and MSI, indicating that targeted therapy may not be suitable in tumors with elevated FBLN5 levels. Overall, FBLN5 exhibits tumor-promoting effects in some cancers, tumor-suppressive effects in others, and supports immunotherapy in some and targeted therapy in others. Therefore, its functional mechanisms should be evaluated individually for each tumor type.

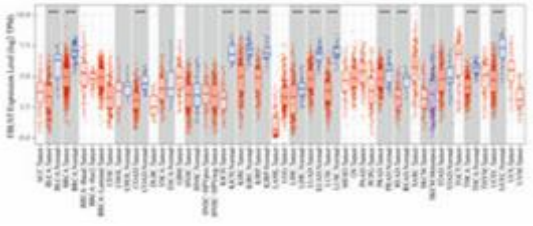

a)

b)

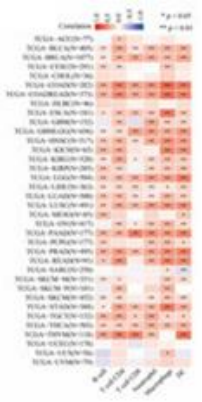

c)

d)

e)

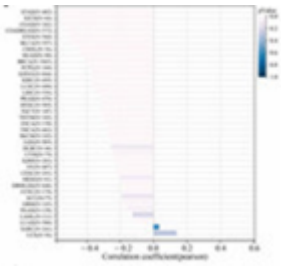

f)

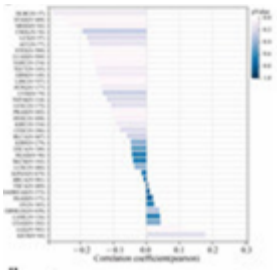

g)

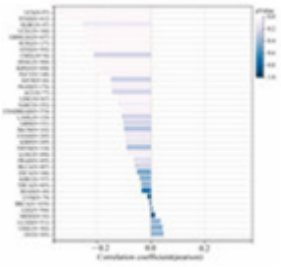

h)

Figure 7. Broader applications of FBLN5 across different malignancies

(a) FBLN5 mRNA expression profiles in multiple tumor types, (b) Survival and outcome analysis associated with FBLN5 in various cancers, (c) TIMER-based and (d) CIBERSORT-based evaluation of links between FBLN5 expression and immune cell infiltration patterns in diverse tumors, (e) Comprehensive pan-cancer assessment of FBLN5 with immune checkpoint expression, supplemented by (f) tumor purity, (g) tumor mutational burden (TMB), and (h) microsatellite instability (MSI) evaluations to determine its viability in targeted therapeutic approaches. * $P < 0.05$, ** $P < 0.01$, *** $P < 0.001$.

Gastric cancer represents one of the most aggressive digestive tract malignancies, featuring a highly intricate tumor microenvironment. Utilizing TCGA-HMU gastric cancer datasets, the current investigation examined the functional contributions of FBLN5 in this disease. Both transcript and protein abundance of FBLN5 were quantified, and their correlations with clinical and pathological parameters as well as overall survival were thoroughly assessed. Results demonstrated that FBLN5 exerts substantial influence within the tumor microenvironment and holds promise as a prognostic indicator tied to fibroblast activity in cancer.

The fibulin family consists of seven extracellular matrix glycoproteins: fibulin-1 through fibulin-7. These molecules regulate key cellular behaviors such as adhesion, motility, and growth, and are commonly found in association with blood vessels and elastic fibers. Individual fibulins are produced by both neoplastic and stromal cells, thereby modulating tumor advancement [26]. FBLN5, produced by fibroblasts, possesses Arg-Gly-Asp (RGD) sequences and calcium-dependent EGF-like repeats. By engaging integrins via its RGD motif, FBLN5 supports endothelial cell attachment. It is indispensable for elastic fiber assembly [14] and participates in blood vessel formation and restructuring [12] as an integrin-binding vascular component. FBLN5 also interacts with TGF-β in both fibroblasts and endothelial cells [16, 17]. Given TGF-β's central role in driving aberrant EMT during fibrotic and oncogenic processes [27, 28], FBLN5 likely contributes meaningfully to cancer development. Recent literature has increasingly highlighted FBLN5's involvement in oncology. For instance, Manders *et al*. [29] demonstrated that FBLN5 activates EMT in a matrix metalloproteinase-dependent manner and intensifies TGF-β-driven EMT in mammary epithelial cells, suggesting its oncogenic properties in breast carcinoma. Likewise, Topalovski *et al*. [21] reported that FBLN5 disrupts fibronectin-integrin interactions, thereby curbing ECM-mediated reactive oxygen species production and accelerating pancreatic cancer progression. Despite these insights, FBLN5's relevance in gastric cancer remained unexplored before this work. We therefore employed the TCGA-HMU resource and tissue microarrays to delineate its clinical implications in GC.

Principal component analysis (PCA) of our datasets revealed strong intra-group clustering, confirming satisfactory sample homogeneity and reproducibility within cohorts. Inter-group separation, however, was modest. This observation likely arises because FBLN5 expression represents a continuous variable, yielding only subtle distinctions between the designated high- and low-expression categories. Notably, elevated FBLN5 levels correlated strongly with advanced T, N, and pTNM stages. Expression intensified alongside greater tumor invasion depth, nodal spread, and overall disease stage, coinciding with inferior clinical outcomes. These patterns position FBLN5 as a potential indicator of progressive disease. Supporting this, Dourado *et al*. [30] established that cancer-associated fibroblast (CAF) density in oral squamous cell carcinoma correlates with multiple adverse prognostic factors, including pTNM stage, histological grade, recurrence risk, and invasion depth, with CAF abundance rising in more advanced

cases. As part of the fibulin family, FBLN5 upregulation in later-stage GC aligns with this dynamic of stromal fibroblasts. Pathway enrichment via KEGG highlighted predominant involvement of the MAPK cascade. In parallel, Li *et al*. [31] observed that depleting ubiquitin-conjugating enzyme E2T (UBE2T) curbs lung adenocarcinoma growth partly by elevating FBLN5, which in turn dampens p-ERK, p-GSK3β, and β-catenin signaling. This implies regulatory interplay between FBLN5 and the MAPK/ERK axis. Furthermore, LOXL1 — an interacting partner of FBLN5 — drives angiogenesis in intrahepatic cholangiocarcinoma through the LOXL1-FBLN5/αvβ3 integrin/FAK-MAPK signaling module [32], thereby facilitating metastatic spread. Such evidence underscores FBLN5's engagement with the RGD-integrin/MAPK pathway during cancer dissemination. GSEA results further linked FBLN5 to TGF-β, EMT, apoptosis, hypoxia, and angiogenic gene sets, reinforcing its multifaceted impact on the tumor milieu and metastatic potential. Consistent with prior reports, FBLN5 promotes EMT and augments TGF-β effects in breast cancer [20], while hypoxia synergizes with TGF-β to induce FBLN5 overexpression in pancreatic cancer, correlating with reduced survival [21]. Yoshida *et al*. [33] additionally established a direct connection between FBLN5 and new vessel formation. Taken together, these mechanisms — hypoxia response, angiogenesis, MAPK activation, EMT induction, and TGF-β signaling — likely underlie the association between FBLN5 overexpression and dismal prognosis in GC patients. Protein-protein interaction mapping identified ELN as a key FBLN5 partner. Earlier findings from our laboratory indicated that ELN mRNA levels correlate with fibroblast markers (especially vimentin) and may predict GC outcomes through EMT modulation [34], suggesting that FBLN5 influences fibroblast behavior.

Barrett and Puré [9] characterized cancer-associated fibroblasts and the extracellular matrix collectively as "stromal" elements that suppress immune effector functions and foster tumor initiation, growth, spread, and resistance to treatment. Because FBLN5 originates from fibroblasts and resides in the extracellular matrix, we propose it may similarly dampen immune responses and promote immune evasion by malignant cells. CIBERSORT profiling revealed pronounced increases in M2-polarized macrophages and dendritic cells within FBLN5-high tumors. Consequently, elevated FBLN5 appears to be associated with the recruitment of immunosuppressive populations, including CAFs, tumor-associated macrophages (TAMs), and dendritic cells. M2 macrophages secrete IL-10, VEGF, and MMPs, promote vessel growth and tissue repair, and exert broad immunosuppressive activity that benefits tumor expansion [35, 36]. Tumor-associated dendritic cells similarly generate factors that expand regulatory T cells and reinforce local immune suppression. Patients with high FBLN5 also showed increased immune, stromal, and ESTIMATE scores, along with decreased tumor purity. We therefore posit that abundant FBLN5 is associated with enhanced fibroblast-driven immunosuppression, warranting further exploration of its interactions with the immune microenvironment.

Clinically, chi-square tests identified significant associations between FBLN5 levels and the INFc growth pattern and N3 nodal status. Zhao *et al*. [37] previously associated the INFc infiltration mode with deeper tumor invasion, immune suppression, and undifferentiated histology — all hallmarks of poor prognosis. Worse survival was also observed with greater lymph node burden. Hence, high FBLN5 may signal advanced-stage disease. Both single-variable and multivariable Cox regression analyses confirmed that FBLN5 expression and the lymph node metastasis rate were independent predictors of GC outcome. The modest number of independent factors detected could reflect the limited cohort (180 cases total, with adequate survival data available for only 100 patients) and the inherently short survival window typical of gastric cancer. Improving long-term follow-up and patient management remains a priority. Integrating FBLN5 expression with lymph node status, we developed a nomogram for individualized prognostic estimation. This model achieved a concordance index of 0.705 (95% CI: 0.659–0.752), with time-dependent AUCs of 0.751 (0.564–0.938) at 1 year, 0.769 (0.647–0.891) at 2 years, and 0.733 (0.612–0.855) at 3 years. Overall, these data underscore FBLN5's translational value in both research and patient care settings.

Pan-cancer bioinformatics further indicated that FBLN5 has favorable prognostic utility in hepatocellular carcinoma. Tang *et al*. [38] reported that reduced FBLN5 expression predicts poorer survival and that FBLN5 restrains hepatocellular carcinoma motility via integrin pathways. Its RGD-dependent suppression of MMP-7 may inspire new treatment modalities. Moreover, FBLN5 levels in tumors such as lung adenocarcinoma (LUAD/STES), bladder transitional cell carcinoma

(BLCA), and lung squamous cell carcinoma (LUSC) may help stratify patients for immunotherapy or targeted agents, supporting tailored strategies that enhance survival and well-being.

Limitations of the current work include the use of gene expression and immunohistochemistry data from separate cohorts, complicating multi-omics integration and cross-validation. The relatively small patient sample size represents another constraint. Finally, although functional validation through cell-based assays is vital for biomarker confirmation, this study relied primarily on computational approaches to assess FBLN5's influence on cell proliferation, migration, and invasiveness.

Conclusion

Collectively, our analyses revealed substantially higher FBLN5 expression in gastric cancer tissues relative to paired non-cancerous adjacent mucosa. Both elevated mRNA and protein levels of FBLN5 were linked to adverse clinical outcomes. High FBLN5 was additionally associated with the INFc infiltration pattern and regional lymph node metastasis. FBLN5 expression, together with lymph node involvement, emerged as independent prognostic factors, enabling the construction of a nomogram for risk stratification. These findings establish FBLN5 as a robust prognostic biomarker in gastric cancer.

Acknowledgments: None

Conflict of Interest: None

Financial Support: None

Ethics Statement: None

References

1. Ajani JA, D'Amico TA, Bentrem DJ, Chao J, Cooke D, Corvera C, et al. Gastric Cancer, Version 2.2022, NCCN Clinical Practice Guidelines in Oncology. J Natl Compr Canc Netw. 2022;20(2):167-92.
2. Digklia A, Wagner AD. Advanced Gastric Cancer: Current Treatment Landscape and Future Perspectives. World J Gastroenterol. 2016;22(8):2403-14.
3. Yang Y, Meng WJ, Wang ZQ. Cancer Stem Cells and the Tumor Microenvironment in Gastric Cancer. Front Oncol. 2021;11:803974.
4. Yago A, Haruta S, Ueno M, Hamada Y, Ogawa Y, Ohkura Y, et al. Adequate Period of Surveillance in Each Stage for Curatively Resected Gastric Cancer: Analyzing the Time and Rates of Recurrence. Gastric Cancer. 2021;24(3):752-61.
5. Unterleuthner D, Neuhold P, Schwarz K, Janker L, Neuditschko B, Nivarthi H, et al. Cancer-Associated Fibroblast-Derived WNT2 Increases Tumor Angiogenesis in Colon Cancer. Angiogenesis. 2020;23(2):159-77.
6. Zhuang J, Lu Q, Shen B, Huang X, Shen L, Zheng X, et al. TGFβ1 Secreted by Cancer-Associated Fibroblasts Induces Epithelial-Mesenchymal Transition of Bladder Cancer Cells through LncRNA-ZEB2NAT. Sci Rep. 2015;5:11924.
7. Oft M, Akhurst RJ, Balmain A. Metastasis Is Driven by Sequential Elevation of H-Ras and Smad2 Levels. Nat Cell Biol. 2002;4(7):487-94.
8. Yan Y, Wang LF, Wang RF. Role of Cancer-Associated Fibroblasts in Invasion and Metastasis of Gastric Cancer. World J Gastroenterol. 2015;21(33):9717-26.
9. Barrett RL, Puré E. Cancer-Associated Fibroblasts and Their Influence on Tumor Immunity and Immunotherapy. eLife. 2020;9:e57243.
10. Timpl R, Sasaki T, Kostka G, Chu ML. Fibulins: A Versatile Family of Extracellular Matrix Proteins. Nat Rev Mol Cell Biol. 2003;4(6):479-89.
11. Argraves WS, Greene LM, Cooley MA, Gallagher WM. Fibulins: Physiological and Disease Perspectives. EMBO Rep. 2003;4(12):1127-31.
12. Nakamura T, Ruiz-Lozano P, Lindner V, Yabe D, Taniwaki M, Furukawa Y, et al. DANCE, a Novel Secreted RGD Protein Expressed in Developing, Atherosclerotic, and Balloon-Injured Arteries. J Biol Chem. 1999;274(32):22476-83.
13. Nakamura T, Lozano PR, Ikeda Y, Iwanaga Y, Hinek A, Minamisawa S, et al. Fibulin-5/DANCE Is Essential for Elastogenesis in Vivo. Nature. 2002;415(6868):171-5.
14. Claus S, Fischer J, Mégarbané H, Mégarbané A, Jobard F, Debret R, et al. A p.C217R Mutation in Fibulin-5 from Cutis Laxa Patients Is Associated with Incomplete Extracellular Matrix Formation in a Skin Equivalent Model. J Invest Dermatol. 2008;128(6):1442-50.
15. Heo JH, Song JY, Jeong JY, Kim G, Kim TH, Kang H, et al. Fibulin-5 Is a Tumour Suppressor Inhibiting

Cell Migration and Invasion in Ovarian Cancer. J Clin Pathol. 2016;69(2):109-16.
16. Schiemann WP, Blobe GC, Kalume DE, Pandey A, Lodish HF. Context-Specific Effects of Fibulin-5 (DANCE/EVEC) on Cell Proliferation, Motility, and Invasion. Fibulin-5 Is Induced by Transforming Growth Factor-Beta and Affects Protein Kinase Cascades. J Biol Chem. 2002;277(30):27367-77.
17. Albig AR, Schiemann WP. Fibulin-5 Antagonizes Vascular Endothelial Growth Factor (VEGF) Signaling and Angiogenic Sprouting by Endothelial Cells. DNA Cell Biol. 2004;23(6):367-79.
18. Hu Z, Ai Q, Xu H, Ma X, Li HZ, Shi TP, et al. Fibulin-5 Is Down-Regulated in Urothelial Carcinoma of Bladder and Inhibits Growth and Invasion of Human Bladder Cancer Cell Line 5637. Urol Oncol. 2011;29(4):430-5.
19. Chen X, Song X, Yue W, Chen D, Yu J, Yao Z, et al. Fibulin-5 Inhibits Wnt/β-Catenin Signaling in Lung Cancer. Oncotarget. 2015;6(17):15022-34.
20. Lee YH, Albig AR, Regner M, Schiemann BJ, Schiemann WP. Fibulin-5 Initiates Epithelial-Mesenchymal Transition (EMT) and Enhances EMT Induced by TGF-Beta in Mammary Epithelial Cells via a MMP-Dependent Mechanism. Carcinogenesis. 2008;29(12):2243-51.
21. Topalovski M, Hagopian M, Wang M, Brekken RA. Hypoxia and Transforming Growth Factor β Cooperate to Induce Fibulin-5 Expression in Pancreatic Cancer. J Biol Chem. 2016;291(43):22244-52.
22. Xiao W, Zhou S, Xu H, Li H, He G, Liu Y, et al. [Corrigendum] Nogo-B Promotes the Epithelial-mesenchymal Transition in HeLa Cervical Cancer Cells via Fibulin-5. Oncol Rep. 2022;47(5):100.
23. Effect of Fibulin-5 on Cell Proliferation and Invasion in Human Gastric Cancer Patients. PubMed [Internet]. 2014 [cited 2022 Dec 30]. Available from: https://pubmed.ncbi.nlm.nih.gov/25129461/
24. Wang X, Zhi Q, Liu S, Xue SL, Shen C, Li Y, et al. Identification of Specific Biomarkers for Gastric Adenocarcinoma by ITRAQ Proteomic Approach. Sci Rep. 2016;6:38871.
25. Shen W, Song Z, Zhong X, Huang M, Shen D, Gao P, et al. Sangerbox: A Comprehensive, Interaction-Friendly Clinical Bioinformatics Analysis Platform. iMeta. 2022;1(3):e36.
26. Obaya AJ, Rua S, Moncada-Pazos A, Cal S. The Dual Role of Fibulins in Tumorigenesis. Cancer Lett. 2012;325(2):132-8.
27. Galliher AJ, Neil JR, Schiemann WP. Role of Transforming Growth Factor-Beta in Cancer Progression. Future Oncol. 2006;2(6):743-63.
28. Nawshad A, Lagamba D, Polad A, Hay ED. Transforming Growth Factor-Beta Signaling during Epithelial-Mesenchymal Transformation: Implications for Embryogenesis and Tumor Metastasis. Cells Tissues Organs. 2005;179(1-2):11-23.
29. Manders DB, Kishore HA, Gazdar AF, Keller PW, Tsunezumi J, Yanagisawa H, et al. Dysregulation of Fibulin-5 and Matrix Metalloproteases in Epithelial Ovarian Cancer. Oncotarget. 2018;9(18):14251-67.
30. Dourado MR, Guerra ENS, Salo T, Lambert DW, Coletta RD. Prognostic Value of the Immunohistochemical Detection of Cancer-Associated Fibroblasts in Oral Cancer: A Systematic Review and Meta-Analysis. J Oral Pathol Med. 2018;47(5):443-53.
31. Li Y, Yang X, Lu D. Knockdown of Ubiquitin-Conjugating Enzyme E2T (UBE2T) Suppresses Lung Adenocarcinoma Progression via Targeting Fibulin-5 (FBLN5). Bioengineered. 2022;13(5):11867-80.
32. LOXL1 Exerts Oncogenesis and Stimulates Angiogenesis through the LOXL1-FBLN5/Avβ3 Integrin/FAK-MAPK Axis in ICC. PubMed [Internet]. 2021 [cited 2022 Oct 29]. Available from: https://pubmed.ncbi.nlm.nih.gov/33614230/
33. Yoshida K, Nagasaka T, Umeda Y, Tanaka T, Kimura K, Taniguchi F, et al. Expansion of Epigenetic Alterations in EFEMP1 Promoter Predicts Malignant Formation in Pancreatobiliary Intraductal Papillary Mucinous Neoplasms. J Cancer Res Clin Oncol. 2016;142(7):1557-69.
34. Fang T, Zhang L, Yin X, Wang Y, Zhang X, Bian X, et al. The prognostic marker elastin correlates with epithelial-mesenchymal transition and vimentin-positive fibroblasts in gastric cancer. J Pathol Clin Res. 2023;9(1):56-72.
35. Belgiovine C, D'Incalci M, Allavena P, Frapolli R. Tumor-Associated Macrophages and Anti-Tumor Therapies: Complex Links. Cell Mol Life Sci. 2016;73(13):2411-24.

36. Pan Y, Yu Y, Wang X, Zhang T. Tumor-Associated Macrophages in Tumor Immunity. Front Immunol. 2020;11:583084.
37. Zhao Y, Xu E, Yang X, Zhang Y, Chen H, Wang Y, et al. Tumor infiltrative growth pattern correlates with the immune microenvironment and is an independent factor for lymph node metastasis and prognosis in stage T1 esophageal squamous cell carcinoma. Virchows Arch. 2020;477(3):401-8.
38. Tang JC, Liu JH, Liu XL, Liang X, Cai XJ. Effect of Fibulin-5 on Adhesion, Migration and Invasion of Hepatocellular Carcinoma Cells via an Integrin-Dependent Mechanism. World J Gastroenterol. 2015;21(38):11127-40.